Biosensors and Bioelectronics 77 (2016) 220–226

Contents lists available at ScienceDirect

Biosensors and Bioelectronics

journal homepage: www.elsevier.com/locate/bios

A versatile immobilization-free photoelectrochemical biosensor for ultrasensitive detection of cancer biomarker based on enzyme-free cascaded quadratic amplification strategy

Lei Ge, Wenxiao Wang, Ting Hou, Feng Li *

College of Chemistry and Pharmaceutical Sciences, Qingdao Agricultural University, Qingdao, Shandong 266109, People's Republic of China

ARTICLE INFO

Article history:
Received 23 July 2015
Received in revised form
17 September 2015
Accepted 18 September 2015

Keywords:
Homogeneous photoelectrochemical assay
Catalytic hairpin assembly
Hybridization chain reaction
DNAzyme
Catalytic precipitation

ABSTRACT

In this work, an ultrasensitive immobilization-free photoelectrochemical (PEC) biosensor was successfully developed for the first time based on a novel enzyme-free cascaded quadratic signal amplification strategy. This rationally designed homogeneous dual amplification strategy consists of a target-analog recycling circuit based on catalytic hairpin assembly (CHA) and a hybridization chain reaction (HCR) mediated amplification circuit. In the presence of carcinoembryonic antigen (CEA), a proof-of-concept target, target-analog is released to trigger the upstream CHA recycling circuit. The generated dsDNA complexes from CHA recycling could further induce the downstream HCR amplification, leading to the formation of numerous hemin/G-quadruplex DNAzymes. This would accordingly stimulate the biocatalytic precipitation of 4-chloro-1-naphthol, inducing a distinct decrease in the photocurrent signal due to the formed insoluble/insulating products on electrode surface. Under the optimal conditions, this PEC biosensor achieved ultrasensitive detection of CEA down to the atto-gram level. The introduction of this aptamer-based cascaded quadratic amplification strategy not only remarkably improves the selectivity and sensitivity of CEA assay, but also allows the ultrasensitive detection of other proteins by designing specific aptamers, providing a universal, isothermal and label-free PEC biosensing platform for ultrasensitive detection of different kinds of cancer biomarkers and holding a great potential for early-diagnosis of cancer.

1. Introduction

It has been recognized that abnormal concentrations of some specific proteins, released from cells and organs, in the circulation system are closely associated with the occurrence and development of cancers (Wu et al., 2007). During the past decades, these specific proteins are widely employed as cancer biomarkers, the levels of which in blood or tissue could provide essential information for cancer diagnosis and monitoring cancer progression (Arya and Bhansali, 2011). As is well-known, in the early stage of cancer, the concentrations of cancer biomarkers are usually on a relatively low level. Therefore, the development of biosensors which are capable of ultra-sensitive profiling trace amounts of cancer biomarkers is not only highly desirable to satisfy the requirement of early diagnosis and medical treatment of cancer, but also plays crucial roles in evaluating the extent of cancer and monitoring its response to therapy. To date, many approaches have been successfully developed for pursuing the exploration of extreme detection sensitivity toward cancer biomarkers (Chikkaveeraiah et al., 2012; Ding et al., 2015; Wu et al., 2007). Among these approaches, photoelectrochemical (PEC) biosensor is a newly emerged approach for the rapid and sensitive detection of cancer biomarkers (Fan et al., 2014; Hu et al., 2013; Li et al., 2013, 2015; Wang et al., 2009; Zeng et al., 2014a, 2014b; Zhang et al., 2014; Zhao et al., 2012a) and has drawn more and more concerns (Yang et al., 2015a, 2015b; Zhao et al., 2014). Coupling photo-excitation with a current readout, PEC biosensors have inherited the advantages from both optical and electrochemical methods (Li et al., 2015; Ma et al., 2015) and offered a promising analytical platform for cancer biomarkers detection with greatly reduced background signals and strikingly improved sensitivity.

However, all the PEC biosensors are implemented through immobilization of bio-recognition probe on the electrode surface. It is well-known that these heterogeneous assays require an appropriate probe-immobilization strategy, which depends greatly on multiple factors. For instance, to obtain good assay performance for target analyte, the orientation and density of the

* Corresponding author.
E-mail address: lifeng@qust.edu.cn (F. Li).

http://dx.doi.org/10.1016/j.bios.2015.09.041
0956-5663/

surface-bounded probes on the modified electrode should be exactly controlled through careful optimizations (Farjami et al., 2012; Lubin et al., 2009; Ricci et al., 2007). In addition, the immobilization processes usually restricted the probe's configurational freedom and even change its geometry due to the steric hindrance effect of the modified electrode surface (Ricci et al., 2007; Yu and Lai, 2013), which results in the much lower binding efficiency and rate between the targets and bio-recognition probes on modified electrode surface than that in solution. Furthermore, the probe-immobilization strategy should vary with the size and configuration of probes, thus no uniform strategy is available for the immobilization of different probes, which may actually limit the routine use of PEC biosensors. Therefore, the elimination of bioprobes immobilization holds great promise in the development of promising PEC strategies.

Another key aspect involved in the achievement of ultrasensitive PEC biosensor is to adopt a signal amplification strategy. DNA recycling amplification strategies, using nucleic acid probes or aptamers as recognition components, has now become powerful tools in the development of various ultrasensitive biosensors (Zhang et al., 2013a) due to its linear or exponential signal amplification capacity. However, in the past decade, very few PEC sensing platforms based on DNA recycling amplification strategies have been proposed, all of which employed tool enzymes as biocatalysts, such as endonucleases (Cao et al., 2014; Shen et al., 2015a; Wang et al., 2014b) terminal deoxynucleotidyl transferase (Shen et al., 2015b), and polymerase (Zhang et al., 2013b; Zhuang et al., 2015). Despite their high sensitivities, these enzyme-based methods encounter the disadvantages of irreversible denaturation of enzymes under harsh conditions. Therefore, the practical applications of these PEC biosensors are greatly limited. In contrast, kinetically favored DNA-activated chain reactions, driven by the free-energy of base pair formation without enzyme, have attracted considerable attention in amplification methods (Wang et al., 2014a). On the other hand, all the aforementioned PEC sensing platforms employ a linear signal amplification strategy, in which only a single DNA-based recycling is designed, limiting the signal enhancement and thus the sensitivity of the assay. During the past several years, cascaded quadratic signal amplification (Duan et al., 2013; Wang et al., 2013; Yu et al., 2014; Zhou et al., 2014) has received considerable attention. Based on this strategy, various cascaded circuit (Jie and Yuan, 2012; Liu et al., 2014; Ma et al., 2014; Yin et al., 2013) were constructed in which the output/product from the first DNA-based recycling acted as the input/trigger for the second DNA-based recycling, leading to an exponential signal amplification.

Hence, in this study, we develop a novel and universal PEC strategy for ultrasensitive detection of cancer biomarker coupling the amplification capability of both catalytic hairpin assembly (CHA) and hybridization chain reaction (HCR) without immobilization of any bioprobe. In the presence of carcinoembryonic antigen (CEA), a proof-of-concept analyte in this work, single-strand trigger-DNA (sstDNA) is released from the CEA-aptamer@sstDNA complex by the target recognition of CEA, initiating the upstream CHA recycling amplification. The upstream products could act as single-strand DNA triggers of the downstream HCR amplification, leading to the formation of the dsDNA nanowires containing numerous hemin/G-quadruplex DNAzymes, which catalyzes the precipitation of 4-chloro-1-naphthol (4-CN) by H_2O_2. The yield insoluble benzo-4-chlorohexadienone in this mimicking-biocatalyzed reaction forms an insulating barrier on the CdS quantum dots (QDs)-TiO_2 nanoparticles (NPs) modified PEC transducer surface, leading to the decrease of photocurrent (Zhao et al., 2012b). Based on this novel cascaded quadratic amplification process, compared to those previous PEC biosensors, the developed versatile and flexible PEC biosensing approach exhibits high specificity and ultra-sensitivity toward detection of biomolecules with trace amounts in clinical biomedicine.

2. Experimental section

2.1. Reagents and apparatus

The reagents and apparatus used in this work are described in Supporting information.

2.2. PEC detection of CEA through the quadratic amplification strategy

Prior to use, all the functional hairpin oligonucleotides were separately refolded into hairpin structures through heating to 95 °C for 3 min and then allowed to slowly cool to room temperature at a rate of 0.01 °C/s. The CEA aptamer (Ap) sequence was previously hybridized with its complementary sstDNA in equal proportions (10.0 μL, 10.0 μM) and incubated at 37 °C for 1 h to obtain the Ap@sstDNA duplex hybrids.

Upon optimizing various conditions, the following procedure was used for the PEC detection with cascaded CHA recycling and HCR amplification. First, Ap@sstDNA solution (3.6 μM, 5.0 μL) and 5.0 μL aliquot of CEA sample solution with different concentrations were mixed in a microcentrifuge tube. After 1 h, 10 μL CHA-hairpins solution (containing 3.0 μM CHA-HP1 and 3.0 μM CHA-HP2) and 10 μL HCR-hairpins solution (containing 4.8 μM HCR-HP1 and 4.8 μM HCR-HP2) were successively added into the above mixture and incubated at room temperature for 2 h and 3 h, respectively. After that, 5.0 μL aliquot of hemin solution containing 6.0 μM hemin and 50 mM KCl was pipetted into the above mixture and incubated for 1 h to form K^+-stabilized G-quadruplex DNAzymes. After incubation, the above mixture was transferred onto the CdS/TiO_2/ITO PEC electrode (Detailed fabrication procedures are shown in Supporting Information), followed by the addition of 5.0 μL aliquot of the precipitation solution containing 0.6 mM H_2O_2 to initiate the G-quadruplex DNAzymes catalyzed precipitation reactions. After 10 min incubation at room temperature, the electrode was rinsed with PBS. Finally, the resulted PEC electrode was introduced to photocurrent intensity (I) measurements, all of which were carried out under 430 nm irradiation (LED light source) at a constant potential of 0.0 V in PBS containing 0.01 M ascorbic acid (AA) as sacrificial electron donor.

2.3. Electrophoresis demonstration of the quadratic amplification strategy

As a further support for this novel quadratic amplification strategy, non-denaturating polyacrylamide gel electrophoresis (PAGE) was employed to verify and characterize its mechanism. Samples containing different DNA structures were added in 1.5 μL 6 × loading buffer, respectively. A 17% native polyacrylamide hydrogel was prepared using 1 × tris–borate–EDTA buffer (TBE, 89 mM Tris Borate, 2.0 mM EDTA, pH 8.3). The above sample mixture was injected into the polyacrylamide hydrogel for electrophoresis. Electrophoresis was carried out at 100 V in TBE buffer for 1 h, and stained for 20 min in a 1 × SYBR Green I solution. The resulting board was then illuminated with ultraviolet light and finally photographed by the gel imaging system.

3. Results and discussion

3.1. Design principle of the PEC biosensor

In this work, a PEC detection system is rational designed to detect CEA with a combination of PEC technology and enzyme-free and immobilization-free cascaded DNA machine amplification strategy, which includes both the CHA recycling circuit and HCR amplification circuit. The principle for PEC detection of CEA based on this novel cascaded quadratic amplification strategy was shown in Fig. 1, and the mechanism of which was also verified by non-denaturating PAGE.

The sequences of CHA-HP1, CHA-HP2, HCR-HP1 and HCR-HP2 were carefully and rationally designed to kinetically hinder any spontaneous interaction between two hairpins in the absence of target input. As illustrated by Fig. 2, each basic DNA structure including Ap (lane-a), sstDNA (lane-b), CHA-HP1 (lane-d), CHA-HP2 (lane-e), HCR-HP1 (lane-g) and HCR-HP2 (lane-h), shows a single and narrow electrophoresis band on both gel board, indicated that no secondary structure is observed in each rationally designed DNA sequence. After the incubation of Ap and sstDNA for 1 h, a new band was displayed in the lane-c on both gel board, confirming the formation of the Ap@sstDNA duplex. Although there are some complementary domains between different DNA structures, mixing all the above DNA structures (lane-f, lane-i and lane-j) in the absence of CEA did not produce any obvious new bands, implying the very low level of spontaneous interactions between each rationally designed DNA structure in the absence of target.

In the presence of CEA (Fig. 2B), Ap@sstDNA complex is dehybridized (lane-k) by the recognition of the aptamer to CEA, resulting in the release of the sstDNA from aptamer (Reaction 1 in Fig. 1) as target analog. Domain-a of the released sstDNA is complementary to domain-a* of CHA-HP1 and acts as a 'toehold' to induce branch migration reaction (Reaction 2), which opens CHA-HP1 and forms the CHA-HP1@sstDNA complex. After that, the occluded domain-c of CHA-HP1 is exposed and serves as a 'toehold' for domain-c* of CHA-HP2 to again initiate branch migration

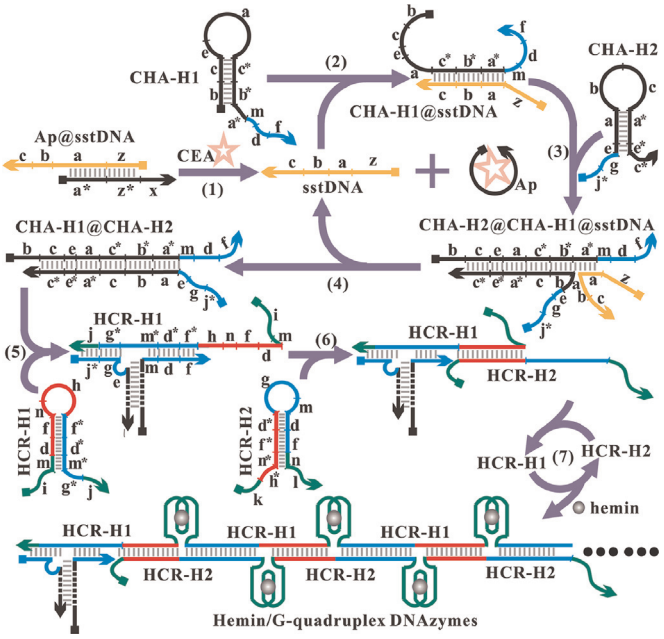

Fig. 1. Schematic illustration of the cascaded quadratic signal amplification strategy for the ultrasensitive PEC detection of CEA. Squares and arrows drawn on DNA strands represent 5′ termini and 3′ termini, respectively.

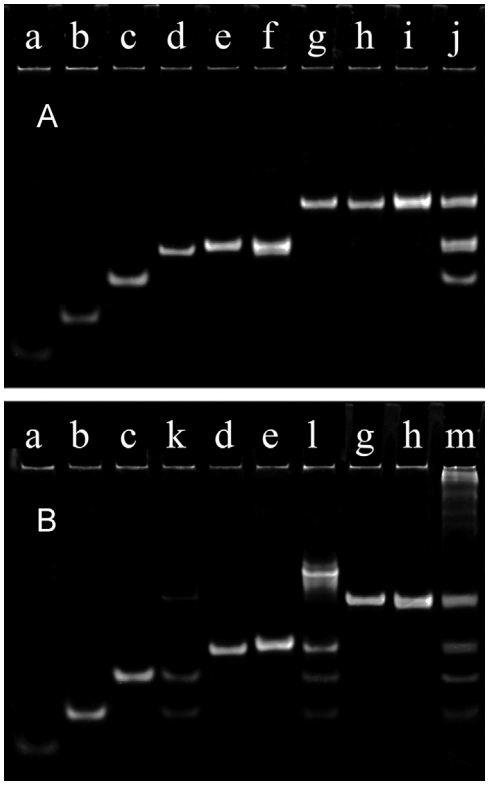

Fig. 2. Native polyacrylamide gel electrophoresis verification of this cascaded quadratic amplification strategy in the absence (Gel board A) and presence (Gel board B) of target CEA. Lane-a: Ap; Lane-b: sstDNA; Lane-c: Ap@sstDNA; Lane-d: CHA-HP1; Lane-e: CHA-HP2; Lane-f: CHA-HP1+CHA-HP2; Lane-g: HCR-HP1; Lane-h: HCR-HP2; Lane-i: HCR-HP1+HCR-HP2; Lane-j: CHA-HP1+CHA-HP2+HCR-HP1+HCR-HP2+Ap@sstDNA; Lane-k: Ap@sstDNA+CEA; Lane-l: CHA-HP1+CHA-HP2+Ap@sstDNA+CEA; Lane-m: CHA-HP1+CHA-HP2+HCR-HP1+HCR-HP2+Ap@sstDNA+CEA.

to form a CHA-HP2@CHA-HP1@sstDNA intermediate (Reaction 3). At the same time, upon branch migration and strand displacement, sstDNA dissociates from the CHA-HP2@CHA-HP1@sstDNA intermediate (Reaction 4), completing the CHA reaction. As illustrated by Fig. 2B, the new band (appears at the minimum electrophoresis distance in lane-l) corresponds to the generated CHA-HP2@CHA-HP1 complexes. It is notable that the brightness of the band corresponding to CHA-HP1 and CHA-HP2 decreases remarkably in lane-l due to the consumption of the two CHA-HPs in CHA recycling circuit, indicates the successful dynamic assembly catalyzed by sstDNA. The released sstDNA (the band at the maximum electrophoresis distance in lane-l) acts as a catalyst and hybridizes again with additional CHA-HP1 to trigger the next CHA recycling process, which will results in the massive production of CHA-HP2@CHA-HP1 complexes.

In this study, as shown in Fig. 1, CHA-HP1 has been extended with an 18 nucleotide (nt) 'branch-migration' segment, containing domain-m, domain-d, and domain-f, at its 3′-end. CHA-HP2 includes a 12 nt 'toehold' segment, containing domain-j* and domain-g, at its 5′-end of the stem region. After CHA reaction, domain-m, domain-d, and domain-f in CHA-HP1 are colocalized with domain-j* and domain-g in CHA-HP2 at the same end of the CHA-HP2@CHA-HP1 duplex complex. This bound 'toehold' and 'branch-migration' segments could then open HCR-HP1 (Reaction 5) (Chen, 2012; Li et al., 2012) through strand displacement, which could further initiate the downstream HCR amplification circuit. The added two bulged thymidines (domain-e) between domain-g and domain-a in CHA-HP2 could not only accelerate this strand

displacement (Chen, 2012), but also stabilize the formed three-way junctions by allowing coaxial stacking of two of the three duplexes (Leontis et al., 1991).

As illustrated in Fig. 1, the autonomous cross-opening of HCR-HP1 and HCR-HP2 (Reactions 6 and 7) in the presence of CHA-HP2@CHA-HP1 duplex complex generated long duplex DNA polymer wire. The new electrophoresis band in lane-m (Fig. 2B) with the slowest gel-shift mobility represents the generated high-molecular weight duplex DNA polymer wire, indicating the successful growth of long double helix. The partially conserved three-fourths of G-quadruplex sequence, encoded at the 5′ or 3′ ends of the two HCR-HPs, are completely exposed and the two split G-quadruplex subunits (green segments in HCR-HPs) are drawn together on the duplex DNA nanowires after HCR-HPs polymerization (Reaction 7) (Shimron et al., 2012). The addition of hemin and K^+ results in the self-assemble of the 3:1 split G-quadruplex subunits into numerous hemin/G-quadruplex peroxidase-mimicking DNAzymes on the duplex DNA nanowires, which are, then, anticipated to catalyze the oxidation of 4-CN by H_2O_2 to insoluble benzo-4-chlorohexadienone, formed an insulating barrier on the CdS/TiO_2/ITO electrode surface (Zhao et al., 2012b; Zhuang et al., 2015), resulting in the decrease of photocurrent. Therefore, a small amount of CEA is expected to efficiently trigger the DNA polymerization and generate numerous hemin/G-quadruplex peroxidase-mimicking DNAzymes for the oxidation of 4-CN, leading to a substantial decrease in the corresponding photocurrent intensity.

3.2. Characterization of the PEC electrode

The stepwise fabrication process of the CdS/TiO_2/ITO electrode and the subsequent precipitation of benzo-4-chlorohexadienone on it were verified by electrochemical impedance spectroscopy (EIS). The redox couple of $[K_3Fe(CN)_6]$/$[K_4Fe(CN)_6]$, which is sensitive to surface chemistry, is used to indicate the electrochemical behaviors of the modified PEC electrode at different stages. The Nyquist diagrams of the modified ITO electrodes at different stages and the corresponding equivalent circuit are displayed in Fig. 3A. The EIS include a semicircle at higher frequencies representing the electron-transfer-limited process and a linear part at lower frequencies resulting from the diffusion-limited process. The semicircle diameter equals the interfacial electron-transfer resistance (R_{et}), which reflects the restricted diffusion of the redox probe accessing the electrode surface. And the R_{et} values can be obtained from fitted results with the equivalent circuit.

For the bare ITO electrode, the impedance spectra exhibited a very small semicircular domain (76.2 Ω). After the successful assemble of TiO_2 NPs film on the surface of ITO electrode, a noticeable increase in R_{et} was observed (180.0 Ω), indicating that the compact TiO_2 NPs film hindered the access of the $[K_3Fe(CN)_6]$/$[K_4Fe(CN)_6]$ redox probe to the ITO electrode surface. The R_{et} value of the CdS/TiO_2/ITO electrode increases to 241.0 Ω on

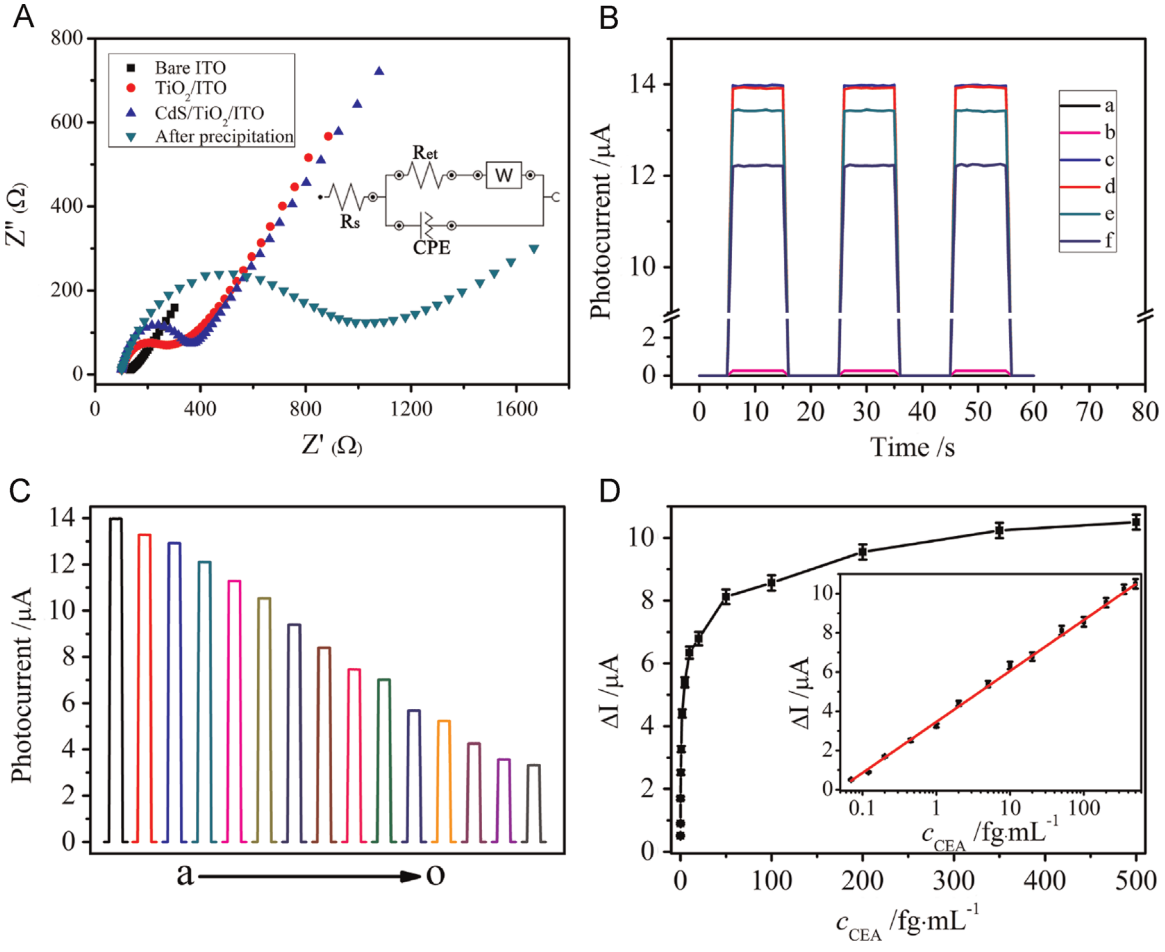

Fig. 3. (A) EIS spectra of the modified PEC electrode at different stages. (B) Photocurrent response of (a) bare ITO electrode, (b) TiO_2/ITO, (c) CdS/TiO_2/ITO, and CdS/TiO_2/ITO electrode upon precipitation of the insoluble/insulating benzo-4-chlorohexadienone at different concentrations of CEA: (d) 0 ag mL^{-1}, (e) 70 ag mL^{-1}, (f) 200 ag mL^{-1}. (C) Photocurrent responses of the proposed PEC biosensor to different concentrations of CEA (from a to o- 0, 0.07, 0.12, 0.2, 0.45, 1.0, 2.0, 5.0, 10, 20, 50, 100, 200, 350 and 500 fg mL^{-1}). (D) Variation of the photocurrent as a function of CEA concentration. Inset: the linear relationship of Δ*I* versus the logarithm of CEA concentration. Error bars showed the standard deviation of eleven experiments.

account of the absorption of semiconductor CdS QDs on TiO_2 NPs films, which blocks the electron communication of ferricyanide with the electrode. In the presence of the substrate 4-CN and H_2O_2, hemin/G-quadruplex peroxidase-mimicking DNAzymes catalyzed precipitation of the insoluble/insulating product onto the CdS/TiO_2/ITO electrode occurred. As expected, the insoluble/insulating precipitation layer not only insulates the electrode surface, but also obstructs the mass transport of the electrochemical probe to the electrode surface, leading to a very high increase in R_{et} (978.0 Ω).

3.3. PEC characterizations

The photocurrent responses from the ITO electrode at different stages with AA as a nontoxic sacrificial electron donor were employed to further confirm the construction process and the feasibility of this PEC biosensor. Fig. 3B showed the photocurrent responses of different modified electrodes. As displayed in curve a, upon irradiation with 430 nm light, no photocurrent response was observed for bare ITO electrode at an applied potential of 0.0 V (curve *a*). A weak photocurrent intensity (curve *b*, I=257.3 nA) was observed on the TiO_2/ITO electrode because that TiO_2 is a wide energy band gap (~3.2 eV) semiconductor material, which can only effectively absorb the ultraviolet light (< 387 nm). Obvious photocurrent was generated (curve *c*, I=13.94 μA) after MPA-capped water-soluble CdS QDs was anchored onto the TiO_2 NPs films. This was attributed to narrower energy band gap (~2.4 eV) of CdS QDs. As illustrated in Fig. S1, the absorption range of CdS QDs can reach to the wavelength of 460 nm. Thus, coupling of CdS QDs with TiO_2 NPs not only extend the absorption range of the modified ITO electrode, but also promote the electron–hole separation in CdS QDs due to the strong electronic coupling effect between the conduction band of CdS QDs and TiO_2 NPs, and thus improve the photocurrent intensity (Wang et al., 2009).

Fig. 3B curves *e* and *f* show the photocurrent responses of the CdS/TiO_2/ITO electrode upon precipitation of the insoluble/insulating benzo-4-chlorohexadienone at different concentrations of CEA. It is evident that as the concentration of CEA is increased, the observed photocurrent response decreases as a result of the precipitation of the benzo-4-chlorohexadienone (curves *e*–*f*). As the insulativity of the formed insoluble precipitation layer on the CdS/TiO_2/ITO electrode surface impedes AA diffusion onto the CdS QDs surface to scavenge the photogenerated holes and thus the photocurrent decreases (Zhao et al., 2012b). This is consistent with the fact that lower concentrations of CEA yield a lesser generation of the CHA-HP2@CHA-HP1 duplex complex in the CHA recycling circuit. This results in lesser formation of the hemin/G-quadruplex peroxidase-mimicking DNAzymes in the HCR amplification circuit, and consequently, a decreased efficiency in the precipitation of the insoluble/insulating benzo-4-chlorohexadienone. Slight photocurrent change was observed (ΔI=48.6 nA) in the absence of CEA (curve *d*), not only suggesting the low background reactivity between different DNA structures in the absence of CEA, but also indicating the low nonspecific adsorption on CdS/TiO_2/ITO electrode as well as the good stability of the as-prepared CdS/TiO_2/ITO electrode. Therefore, the photocurrent responses could serve as the quantitative signal for the CEA determination.

3.4. Sensitivity of this PEC biosensor

To evaluate the sensitivity of the proposed PEC strategy, CEA sample solutions with different concentrations were measured under the optimized experimental concentrations (Detail optimizations are shown in Supporting information) based on the developed quadratic amplification strategy. For each CEA concentration, the PEC measurement was repeated eleven times independently. It can be seen in Fig. 3C that the generated photocurrents decreased along with the increase of CEA concentration, indicating that the formation of insoluble/insulating precipitation was highly dependent on the concentration of CEA.

This also further verified the working principle that the CEA was recognized by the Ap@sstDNA to trigger the DNAzymes catalyzed precipitation. As illustrated in Fig. 3D, the ΔI was found to be logarithmically related to the CEA concentrations in the range from 70 ag mL^{-1} to 500 fg mL^{-1}. $\Delta I = I_0 - I$, where I_0 and I are the photocurrents of biosensor without and with target CEA, respectively. The inset in Fig. 3D displayed the linear relationship between ΔI and the logarithm of CEA concentrations. The linear regression equations were expressed as $\Delta I(\mu A) = 2.599 \lg[c_{CEA}(\text{fg mL}^{-1})] + 3.459$ (r=0.9965). The directly measured detection limit for CEA was obtained at 70 ag mL^{-1}, which is superior or comparable to those of other previously reported biosensors for CEA. The detailed comparison of the proposed PEC strategy with others was illustrated in Table S3. The ultra-sensitivity of the proposed PEC strategy might be attributed to (i) the high amplification efficiency of the coupled CHA and HCR recycling amplification circuits mediated by the programmable DNA structures in homogeneous solution phase, which enabled the conversion of a trace amount of CEA to a large number of peroxidase-mimicking DNAzymes, (ii) the rationally designed sequences of the DNA structures can remarkably minimize the background interaction, and (iii) the integration of cascaded quadratic amplification strategy with sensitive PEC detection. The low detection limit allows ultrasensitive and accurate quantitation of cancer biomarkers at low concentrations, which is of great significance in the early-diagnosis of cancers.

To further confirm the cascaded quadratic signal amplification effect of the currently proposed strategy, CHA-HP3 and CHA-HP4 were designed as a substitute of CHA-HP1 and CHA-HP2 for comparison respectively (Table S1). Domain-j at the 3′ end of CHA-HP3 consists of one-fourth of the G-quadruplex sequence. Domain-m and domain-i at its 5′ end of CHA-HP4 include the encoded sequence that consists of three-fourths of the G-quadruplex sequence. The fact that domain-m is hybridized with domain-m* of the stems in CHA-HP4, which prevents the self-assembly of the active hemin/G-quadruplex DNAzyme between CHA-HP3 and CHA-HP4 in absence of CEA. It is notable that the sequences of domain-a, domain-b, and domain-c in CHA-HP3 and CHA-HP4 remained unchanged. That is, as shown in Fig. 4A, the release of sstDNA after CEA recognition by Ap@sstDNA could also trigger the cross-opening of the CHA-HP3 and CHA-HP4 and resulted in the formation of the CHA-HP3@CHA-HP4 complex, but no further HCR amplification circuit could be initiated. Thus, one CHA-HP3@CHA-HP4 complex structure could only induce the generation of one active hemin/G-quadruplex DNAzyme through drawing the 3:1 split G-quadruplex fragments together. This CHA-based single-recycling amplification strategy was then explored for the detection of CEA with different concentrations (Fig. 4B). The PEC responses increased linearly with the logarithm of CEA concentrations in 4 orders of magnitude from 8.0 fg mL^{-1} to 50.0 pg mL^{-1} CEA (Fig. 4C). The directly measured detection limit for CEA based on this single amplification strategy was obtained at 8.0 fg mL^{-1}, which is 2 orders of magnitude higher than that of quadratic amplification strategy. Also, it should be noted that the PEC responses to CEA by the cascaded quadratic amplification strategy at the same concentrations was significantly lower than that by the CHA-based single-recycling amplification strategy, indicating the higher signal amplification efficiency of the cascaded quadratic amplification strategy.

3.5. Selectivity and reproducibility of the PEC biosensor

To assess the specificity of the proposed PEC biosensing strategy, a series of contrast experiments were performed to evaluate

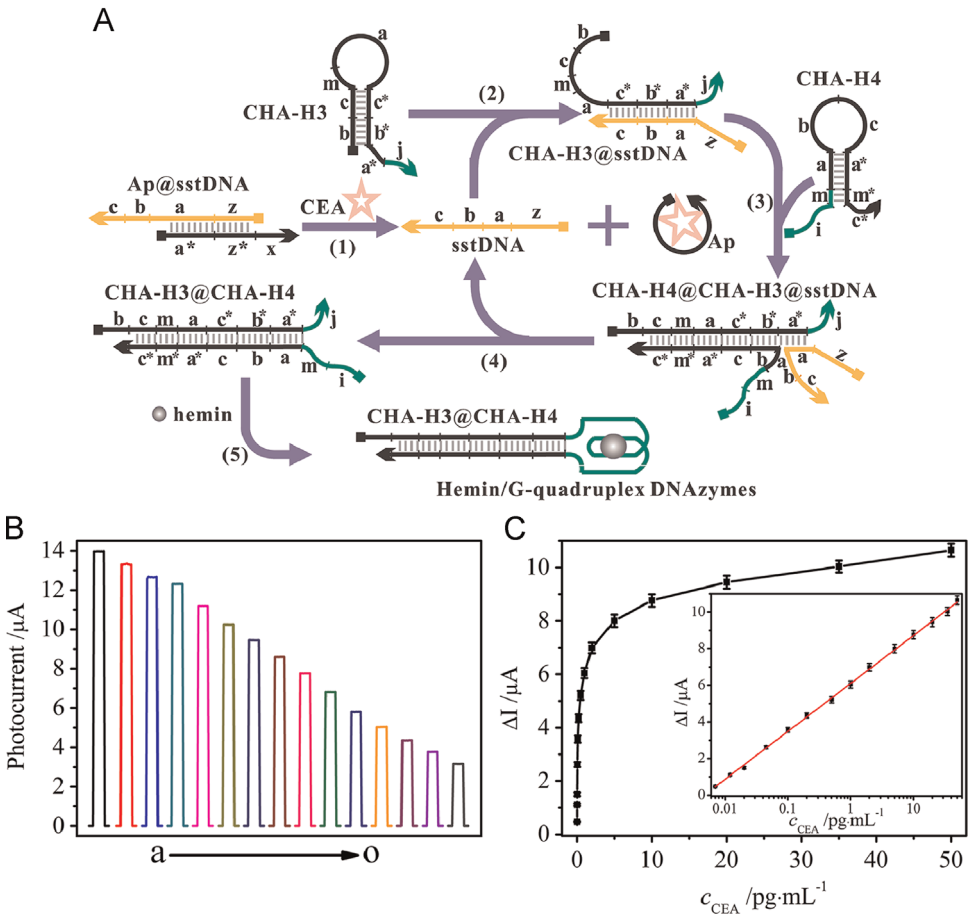

Fig. 4. (A) Schematic illustration of the CHA-based single-recycling amplification strategy. (B) Photocurrent response of (A) to different concentrations of CEA (from a to o- 0, 0.008, 0.012, 0.02, 0.045, 0.1, 0.2, 0.5, 1.0, 2.0, 5.0, 10, 20, 35 and 50 pg mL^{-1}). (C) Variation of the photocurrent as a function of CEA concentration. Inset: the linear relationship of ΔI versus the logarithm of CEA concentration. Error bars showed the standard deviation of eleven experiments.

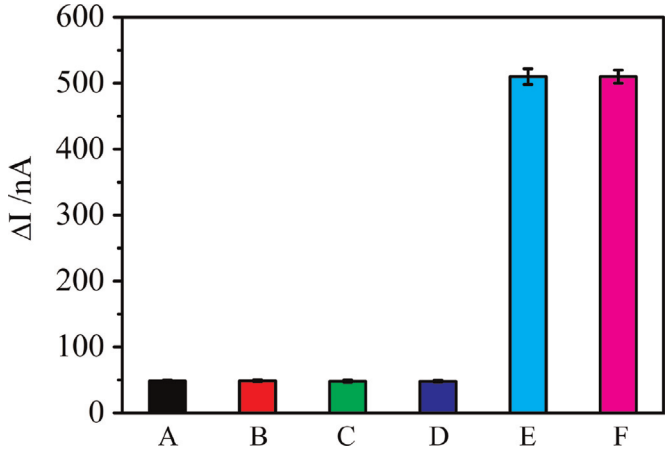

Fig. 5. Selectivity of this PEC biosensor. (A) Blank; (B) 10 ng mL^{-1} AFP; (C) 10 ng mL^{-1} CA125; (D) 10 ng mL^{-1} CA199; (E) 70 ag mL^{-1} CEA sample coexisted with 10 ng mL^{-1} AFP, 10 ng mL^{-1} CA125, and 10 ng mL^{-1} CA199; (F) 70 ag mL^{-1} CEA.

the influences of some other cancer biomarkers such as alpha-fetoprotein (AFP), carcinoma antigen 125 (CA125), carcinoma antigen 199 (CA199) under the same experimental conditions using a sample without CEA as a blank control. The results in Fig. 5 showed that none of these cancer biomarkers caused obvious photocurrent alteration even with a concentration as high as 10 ng mL^{-1}, while the photocurrent from only 70 ag mL^{-1} CEA scarcely decreased compared with the blank control, indicating those cancer biomarkers did not interfere with the CEA detection. Similarly, a 70 ag mL^{-1} CEA sample coexisted with 10 ng mL^{-1} AFP, 10 ng mL^{-1} CA125, and 10 ng mL^{-1} CA199 does not exhibit photocurrent change compared with that of CEA alone. The good specificity to discriminate CEA and other cancer biomarkers gave this PEC detection strategy great potential for accurate early-diagnosis of cancers.

The reproducibility of this proposed PEC biosensor was investigated based on interassay precision between 10 PEC biosensors (measurements of the same sample on 10 different PEC biosensors prepared in different batches). The relative standard deviations for the parallel detection of 0, 70 ag mL^{-1}, and 20 fg mL^{-1} CEA with 10 PEC biosensors, respectively, were 3.24%, 3.91%, and 3.75%. To investigate the stability of this PEC biosensor, it was stored in dark condition at 4 °C and measured at intervals of 3 days; no obvious photocurrent change was observed after 4 weeks. These results indicated that this PEC biosensor had good reproducibility and was fairly robust in normal storage conditions and achieved sufficient stability and precision during manufacture, storage, or long-distance transport.

3.6. Real sample analysis of CEA

The practical applicability and validity of the proposed PEC biosensing strategy was verified through the detection of CEA in five human serum samples, which were appropriately diluted with PBS prior to assay. The assay results obtained by this method were compared with those obtained by the commercially used electrochemiluminescence method in tumor hospitals. The results

Table 1
Assay results of real human serum by the proposed and reference method.

Samples	CEA concentration (ng mL^{-1})		
	Proposed method	Reference method	Relative error (%)
Sample-1	2.42	2.47	−2.03
Sample-2	6.65	6.51	2.15
Sample-3	3.93	3.86	1.81
Sample-4	9.01	9.17	−1.74
Sample-5	17.28	17.62	−1.93

were shown in Table 1. The proposed PEC biosensing strategy showed an acceptable agreement with the reference method. These results suggest that the PEC method may be competent for monitoring real samples.

4. Conclusions

In summary, taking advantages of the biocatalytic precipitation-based PEC biosensor in combination with a novel enzyme-free cascaded quadratic signal amplification strategy, we developed a versatile immobilization-free PEC biosensing approach for the first time, which enables the isothermal and label-free CEA detection with ultrahigh sensitivity. To the best of our knowledge, the present work is also the first attempt to integrate the amplification capability of both CHA and HCR circuit. More specifically, unlike the existing PEC biosensors, the proposed PEC platform enables the target recognition as well as the amplification reactions to occur in a homogeneous solution phase instead of on the electrode/solution interface, endowing the proposed PEC strategy with improved recognition/reaction efficiency compared with heterogeneous PEC biosensor. Furthermore, this proposed PEC approach can be programmed in ways to offer unique advantages and capabilities. First of all, it is notable that, to detect different cancer markers, we just need to change sequences of domain-a/a* and domain-z in the sstDNA and CHA-HPs according to the sequence of target's aptamer. For the signal transduction element, the ingeniously and rationally designed sequence and structure of DNA complexes or hairpins not only facilitates the signal amplification efficiency, but also inhibits the background reaction. Second, the proposed protocol showed a broad dynamic range and achieved ultrasensitive PEC detection of CEA down to the atto-gram level by introducing coupled CHA and HCR to realize quadratic amplification, which could be used for many other detection platforms, such as colorimetry, fluorescence, or chemiluminescence.

Acknowledgments

This work was financially supported by National Natural Science Foundation of China (Nos. 31501570, 21445002, 21575074); Natural Science Foundation of Shandong Province (ZR2014BQ011); Research Foundation for Distinguished Scholars of Qingdao Agricultural University (663-1115003).

Appendix A. Supplementary material

Supplementary data associated with this article can be found in the online version at http://dx.doi.org/10.1016/j.bios.2015.09.041.

References

Arya, S.K., Bhansali, S., 2011. Chem. Rev. 111, 6783–6809.
Cao, H., Liu, S., Tu, W., Bao, J., Dai, Z., 2014. Chem. Commun. 50, 13315–13318.
Chen, X., 2012. J. Am. Chem. Soc. 134, 263–271.
Chikkaveeraiah, B.V., Bhirde, A.A., Morgan, N.Y., Eden, H.S., Chen, X., 2012. ACS Nano 6, 6546–6561.
Ding, C., Zhang, W., Wang, W., Chen, Y., Li, X., 2015. TrAC, Trends Anal. Chem. 65, 137–150.
Duan, R., Zuo, X., Wang, S., Quan, X., Chen, D., Chen, Z., Jiang, L., Fan, C., Xia, F., 2013. J. Am. Chem. Soc. 135, 4604–4607.
Fan, G.-C., Han, L., Zhu, H., Zhang, J.-R., Zhu, J.-J., 2014. Anal. Chem. 86, 12398–12405.
Farjami, E., Campos, R., Ferapontova, E.E., 2012. Langmuir 28, 16218–16226.
Hu, C., Zheng, J., Su, X., Wang, J., Wu, W., Hu, S., 2013. Anal. Chem. 85, 10612–10619.
Jie, G., Yuan, J., 2012. Anal. Chem. 84, 2811–2817.
Leontis, N.B., Kwok, W., Newman, J.S., 1991. Nucleic Acids Res. 19, 759–766.
Li, B., Jiang, Y., Chen, X., Ellington, A.D., 2012. J. Am. Chem. Soc. 134, 13918–13921.
Li, H., Mu, Y., Yan, J., Cui, D., Ou, W., Wan, Y., Liu, S., 2015. Anal. Chem. 87, 2007–2015.
Li, Y.-J., Ma, M.-J., Yin, G., Kong, Y., Zhu, J.-J., 2013. Chem. Eur. J 19, 4496–4505.
Liu, S., Lin, Y., Wang, L., Liu, T., Cheng, C., Wei, W., Tang, B., 2014. Anal. Chem. 86, 4008–4015.
Lubin, A.A., Vander Stoep Hunt, B., White, R.J., Plaxco, K.W., 2009. Anal. Chem. 81, 2150–2158.
Ma, F., Yang, Y., Zhang, C.-y, 2014. Anal. Chem. 86, 6006–6011.
Ma, W., Wang, L., Zhang, N., Han, D., Dong, X., Niu, L., 2015. Anal. Chem. 87, 4844–4850.
Ricci, F., Lai, R.Y., Heeger, A.J., Plaxco, K.W., Sumner, J.J., 2007. Langmuir 23, 6827–6834.
Shen, Q., Han, L., Fan, G., Abdel-Halim, E.S., Jiang, L., Zhu, J.-J., 2015a. Biosens. Bioelectron. 64, 449–455.
Shen, Q., Han, L., Fan, G., Zhang, J.R., Jiang, L., Zhu, J.J., 2015b. Anal. Chem. 87, 4949–4956.
Shimron, S., Wang, F., Orbach, R., Willner, I., 2012. Anal. Chem. 84, 1042–1048.
Wang, F., Freage, L., Orbach, R., Willner, I., 2013. Anal. Chem. 85, 8196–8203.
Wang, F., Lu, C.-H., Willner, I., 2014a. Chem. Rev. 114, 2881–2941.
Wang, G.-L., Xu, J.-J., Chen, H.-Y., Fu, S.-Z., 2009. Biosens. Bioelectron. 25, 791–796.
Wang, W., Hao, Q., Wang, W., Bao, L., Lei, J., Wang, Q., Ju, H., 2014b. Nanoscale 6, 2710–2717.
Wu, J., Fu, Z., Yan, F., Ju, H., 2007. TrAC, Trends Anal. Chem. 26, 679–688.
Yang, J., Gao, P., Liu, Y., Li, R., Ma, H., Du, B., Wei, Q., 2015a. Biosens. Bioelectron. 64, 13–18.
Yang, Z., Wang, F., Wang, M., Yin, H., Ai, S., 2015b. Biosens. Bioelectron. 66, 109–114.
Yin, B.-C., Liu, Y.-Q., Ye, B.-C., 2013. Anal. Chem. 85, 11487–11493.
Yu, Y., Chen, Z., Shi, L., Yang, F., Pan, J., Zhang, B., Sun, D., 2014. Anal. Chem. 86, 8200–8205.
Yu, Z.-g., Lai, R.Y., 2013. Anal. Chem. 85, 3340–3346.
Zeng, X., Bao, J., Han, M., Tu, W., Dai, Z., 2014a. Biosens. Bioelectron. 54, 331–338.
Zeng, X., Tu, W., Li, J., Bao, J., Dai, Z., 2014b. ACS Appl. Mater. Interfaces 6, 16197–16203.
Zhang, H., Li, F., Dever, B., Li, X.-F., Le, X.C., 2013a. Chem. Rev. 113, 2812–2841.
Zhang, X., Liu, M., Mao, Y., Xu, Y., Niu, S., 2014. Biosens. Bioelectron. 59, 21–27.
Zhang, X., Xu, Y., Zhao, Y., Song, W., 2013b. Biosens. Bioelectron. 39, 338–341.
Zhao, W.-W., Ma, Z.-Y., Yan, D.-Y., Xu, J.-J., Chen, H.-Y., 2012a. Anal. Chem. 84, 10518–10521.
Zhao, W.-W., Ma, Z.-Y., Yu, P.-P., Dong, X.-Y., Xu, J.-J., Chen, H.-Y., 2012b. Anal. Chem. 84, 917–923.
Zhao, W.-W., Xu, J.-J., Chen, H.-Y., 2014. Chem. Soc. Rev. 44, 729–741.
Zhou, W., Gong, X., Xiang, Y., Yuan, R., Chai, Y., 2014. Anal. Chem. 86, 953–958.
Zhuang, J., Lai, W., Xu, M., Zhou, Q., Tang, D., 2015. ACS Appl. Mater. Interfaces 7, 8330–8338.